Design of In[sub x]Ga[sub 1−x]As[sub 1−y]N[sub y]∕AlAs quantum cascade structures for 3.4 μm intersubband emission

Dang, Y. X.; Fan, Weijun

Design of In$_x$Ga$_{1-x}$As$_{1-y}$N$_y$/AlAs quantum cascade structures for 3.4 μm intersubband emission

Y. X. Dang and W. J. Fan[a)]

School of Electrical and Electronic Engineering, Nanyang Technological University,
Singapore 639798, Singapore

We report the design of an active region of In$_x$Ga$_{1-x}$As$_{1-y}$N$_y$/AlAs quantum cascade laser structure emitting in the near infrared wavelength range based on an eight-band $k \cdot p$ model. The In$_x$Ga$_{1-x}$As$_{1-y}$N$_y$/AlAs heterostructure system is of significant interest for the development of short wavelength quantum cascade lasers due to its large conduction band discontinuity ($\sim$1.5 eV) and compatibility with the mature GaAs fabrication process. A detailed analysis of the intersubband transition energy within the conduction band as a function of layer thickness, composition, electric field, and temperature has been carried out. Finally, an optimized combination of In$_{0.2}$Ga$_{0.8}$As$_{0.97}$N$_{0.03}$/AlAs three-coupled-well structure has been obtained. Under an applied field of 100 kV/cm and at room temperature, a shortest wavelength of 3.4 μm has been achieved by making use of this system without introducing an upper lasing level beyond the X minima of the AlAs barrier. © 2007 American Institute of Physics. [DOI: 10.1063/1.2717130]

I. INTRODUCTION

Ever since the first quantum cascade lasers (QCLs) were demonstrated by a team of researchers at Bell Labs,[1] tremendous progress in QCL research has resulted in applications such as ultrawide tunable sources, femtosecond-pulse mode locking, second-harmonic generation, and trace gas detection. In the early stage, the main material system used for the realization of QCLs was in the InP based InGaAs–AlInAs system,[1] and a significant improvement of the device performance such as continuous wave (cw) operations above 5 μm at room temperature has been demonstrated since.[2,3] However, there has been no report of such high performance laser operation in the technologically important $\lambda \sim 3 - 5$ μm atmospheric window region by utilizing the same system. The obstacle in obtaining the short wavelength QCL operation originates from the relatively small conduction band offset (CBO) of the InGaAs-AlInAs heterostructure ($\sim$520 meV). Consequently, the main challenge of the $3 - 5$ μm QCL design is to seek material systems with the highest possible CBO. Recently, the InGaAs–AlAsSb heterostructures grown on the InP substrates with CBO up to 1.6 eV have been extensively studied,[4] and a QCL emitting at $\lambda \sim 4.5$ μm up to at least 400 K in pulsed mode has been achieved.[5] Another promising system for the development of QCLs is InAs–AlSb (CBO $\sim$2.1 eV) grown on GaSb or InAs substrates. $3.5 - 5.5$ μm emissions have been reported by utilizing this heterostructure grown on a GaSb substrate;[6] however, no stable laser devices on such a specific substrate can be produced up to now.

In comparison with the systems discussed above, traditional GaAs based GaAs–Al(Ga)As system offers more growth flexibility. QCLs based on this system have been under extensive research for the past decade. A GaAs–AlGaAs QCL with emission at 9.4 μm was realized in 1998,[7] since then the radiation wavelengths of QCLs have been extended to as long as 160 μm.[8] However, a QCL emitting below 5 μm has not been achieved with this system. The limitation is set by the well depth of the GaAs–AlGaAs heterostructure. With up to 33% Al content, the conduction band discontinuity is no more than 0.3 eV. Though the GaAs–AlAs system has a much larger CBO ($\sim$1 eV), the effective CBO in the GaAs/AlAs heterostructure is much smaller ($\sim$0.2 eV) in consideration of the Γ-X indirect discontinuity. Yet the emission wavelengths below 5 μm with the GaAs/AlAs heterosturcture are hard to achieve.[9] For applications of free space communications, stable laser devices emitting at the atmospheric transparent window are highly desirable. It leads to the design of active regions with as deep a well as one can obtain on the GaAs substrates.

If we restrict ourselves on GaAs based systems, a promising way to satisfy the requirements is by utilizing the In$_x$Ga$_{1-x}$As$_{1-y}$N$_y$/AlAs heterosystems for the QCL active region design. Though there is no demonstration of intersubband emissions in the InGaAsN–AlAs systems to date, the intersubband transitions in the In$_{0.3}$Ga$_{0.7}$As/AlAs heterostructures at a wavelength as short as 1.26 μm have been observed.[10] In addition to that, by adding a small amount of nitrogen atoms into the In$_x$Ga$_{1-x}$As matrix to form the In$_x$Ga$_{1-x}$As$_{1-y}$N$_y$ alloy, it was found to greatly reduce the band-gap energy and simultaneously reduce the compressive strain introduced in the well layer.[11] Moreover, the incorporation of N content will exclusively affect the conduction band edge, while leaving the valence band edge untouched. With the same concentration of indium, the CBO of the heterostructure is to increase by more than 200 meV with only 2% N content being introduced.[12] Due to its large CBO ($\sim$1.5 eV), electrons being thermally activated into continuum states can be considerably suppressed, which results in the improvement of the temperature dependent threshold current characteristics.[13] In this work, we report a QCL ac-

a)Electronic mail: ewjfan@ntu.edu.sg

tive region design based on GaAs substrates in order to achieve the goal of $3-5$ μm laser emissions.

II. METHOD

A. Basic theory for intersubband transitions in QCL

The concentration of the QCL structure design is to optimize the active region. In this work, we only consider the most conventional three-quantum-well (TQW) type, which includes a three-level transition system, in which, level 3 (E_3) is the upper lasing level, level 2 (E_2) is the lower lasing level, and level 1 (E_1) is the ground level in the active region. The laser scheme makes use of the three discrete electronic states confined in the QWs. Electrons make radiative transitions from E_3 to E_2, which corresponds to the desired emission wavelengths. Subsequently, the intersubband transition energy between E_2 and E_1 is made equal to the optical phonon energy, which inducing the electrons in E_2 quickly transits to E_1. Therefore the maximized population inversion between E_3 and E_2 is established. In short, our aim is to design a coupled quantum well (CQW) structure with $E_3 - E_2 =$ the lasing transition energy and $E_2 - E_1 =$ the optical phonon energy of the well layer.

B. Band structure calculation

The eigenstates of the QC structures satisfy the Schrödinger equation

$$H\Phi = E\Phi, \tag{1}$$

where Φ is the total wave function. Within the framework of the eight-band $k \cdot p$ model, the eight dimensional electron and hole envelope wave functions for the quantum wells are written as

$$\Phi_n = \{\Phi_n^j\} \quad (j = 1, 2, \ldots, 8), \tag{2}$$

where the components of Φ_n^j are given by

$$\Phi_n^j = \exp[i(k_x x + k_y y)] \sum_m a_{n,m}^j \frac{1}{\sqrt{L}} \exp\left[i\left(k_z + m\frac{2\pi}{L}\right)z\right], \tag{3}$$

where $L = ww1 + ww2 + ww3 + bw1 + bw2 + bw3$ designates the periodicity of the CQW. We use ww1, ww2, and ww3 to indicate the widths of quantum wells and bw1, bw2, and bw3 to represent the widths of barrier layers, respectively, as illustrated in Fig. 1. k_x, k_y, and k_z are the wave vectors. n is the index for energy levels, $a_{n,m}^j$ is the expansion coefficient, and z is the coordinate in the growth direction.

The eight-band $k \cdot p$ method was previously applied by us to calculate dilute nitride related alloys, such as InGaAsN, (Refs. 11 and 14) GaAsSbN,[15] and the results show the reliability of this method. The complete $8 \times 8 k \cdot p$ Hamiltonian and the solution of Eq. (1) can be traced throughout our earlier work. Though the model was only applied to the calculations on the single QW cases before, utilizing it in the calculations of CQW structure is straightforward. One only needs to redefine the period L of the CQW along the growth direction, as mentioned previously. Except for the band-gap energies and electron effective masses, most parameters for
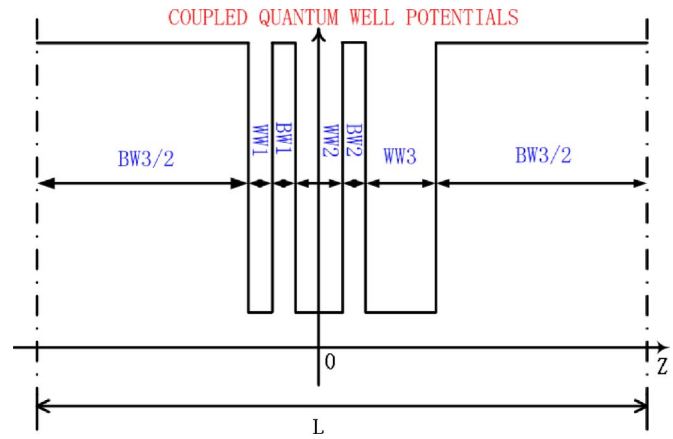

FIG. 1. (Color online) Schematic conduction band potential diagram of one period of the active region of the laser core. L is the length of one period along the growth direction z. ww1 to ww3 denote the well widths of the first well to the last well and bw1 to bw3 denote the barrier widths of the first barrier to the last barrier. The zero point is taken at the center point of the second well. Hereinafter, we applied the same definitions to perform calculations.

In$_x$Ga$_{1-x}$As$_{1-y}$N$_y$ materials are obtained using a linear interpolation between the parameters of the relevant binary compounds, which can be expressed as

$$P(In_x Ga_{1-x} As_{1-y} N_y)$$
$$= P(GaAs)(1-x)(1-y) + P(InAs)x(1-y)$$
$$+ P(GaN)(1-x)y + P(InN)xy. \tag{4}$$

The parameters used are shown in Table I.[16,17] The band-gap energy of In$_x$Ga$_{1-x}$As$_{1-y}$N$_y$ is calculated by the band anticrossing (BAC) model following Ref. 14, which we write in the following form:

$$E_g(In_x Ga_{1-x} As_{1-y} N_y)$$
$$= \{E_g(In_x Ga_{1-x} As) + E^N$$
$$- \sqrt{[E_g(In_x Ga_{1-x} As) - E^N]^2 + 4V^2(1-y)}\}/2, \tag{5}$$

where

TABLE I. Parameters for binary compounds used in the calculation.

Parameters	GaAs[a]	InAs[a]	GaN[b]	InN[b]
Lattice constant a_0 (Å)	5.6533	6.0584	4.5000	4.9800
Spin-orbit splitting energy Δ_0 (eV)	341	390	17	5
Optical matrix parameter E_p (eV)	28.8	21.5	25.0	17.2
Deformation potential constant a_c (eV)	−7.17	−5.08	−6.71	−2.65
Deformation potential constant a_v (eV)	1.16	1.00	0.69	0.70
Shear deformation potential b (eV)	−2.0	−1.8	−2.0	−1.2
Elastic constant c_{11} (GPa)	122.10	83.29	293.00	187.00
Elastic constant c_{12} (GPa)	56.60	45.26	159.00	125.00
Luttinger parameter γ_1	6.98	20.00	2.70	3.72
Luttinger parameter γ_2	2.06	8.50	0.76	1.26
Luttinger parameter γ_3	2.93	9.20	1.11	1.63
Conduction band effective mass m_e^* (m_0)	0.067	0.026	⋯	⋯
Unstrained band-gap energy E_g ($T=300$ K) (eV)	1.422	0.354	⋯	⋯

[a]Reference 16.
[b]Reference 17.

$$E_g(\text{In}_x\text{Ga}_{1-x}\text{As}) = (1-x)[E_g(\text{GaAs},T)] + x[E_g(\text{InAs},T)] - 0.477(1-x), \tag{6}$$

with temperature (T) being taken into account and the band-gap energy is in unit of eV. And the effective masses m_e^* as predicted by the BAC model are given by

$$m_e^*(\text{In}_x\text{Ga}_{1-x}\text{As}_{1-y}\text{N}_y) = 2m_e^*(\text{In}_x\text{Ga}_{1-x}\text{As}) \left/ \left\{ 1 - \frac{E_g(\text{In}_x\text{Ga}_{1-x}\text{As}) - E^N}{\sqrt{[E_g(\text{In}_x\text{Ga}_{1-x}\text{As}) - E^N]^2 + 4V^2 y}} \right\}, \right. \tag{7}$$

where we have

$$m_e^*(\text{In}_x\text{Ga}_{1-x}\text{As}) = (1-x)m_e^*(\text{GaAs}) + xm_e^*(\text{InAs}) - 0.0091x(1-x). \tag{8}$$

Note that the bowing factors 0.477 and 0.0091 in Eqs. (6) and (8), respectively, are recommended by Ref. 16. Calculations of BAC parametrized variables, E^N and V, are presented in Ref. 11. Another important parameter which will strongly affect the results of the calculations is the CBO ratio (Q_c). Thanks to the special characteristic of nitrogen atoms, a small amount of nitrogen incorporated only affects the conduction band edge of the $\text{In}_x\text{Ga}_{1-x}\text{As}_{1-y}\text{N}_y$/AlAs heterosystem. Though there are no reports on the values of Q_c in the $\text{In}_x\text{Ga}_{1-x}\text{As}_{1-y}\text{N}_y$/AlAs QWs up to now, we propose the derivation of these values from that of the extensively researched $\text{In}_x\text{Ga}_{1-x}\text{As}$/AlAs QWs.[18] Thus, the explicit expression for Q_c is given by

$$Q_c(\text{In}_x\text{Ga}_{1-x}\text{As}_{1-y}\text{N}_y/\text{AlAs}) = 1 - Q_v(\text{In}_x\text{Ga}_{1-x}\text{As}_{1-y}\text{N}_y/\text{AlAs}) = 1$$
$$- \frac{\Delta E_g^s(\text{In}_x\text{Ga}_{1-x}\text{As}/\text{AlAs})Q_v(\text{In}_x\text{Ga}_{1-x}\text{As}/\text{AlAs}) + \Delta_v^s(\text{In}_x\text{Ga}_{1-x}\text{As}/\text{In}_x\text{Ga}_{1-x}\text{As}_{1-y}\text{N}_y)}{E_{g\_\text{AlAs}}^s - E_{g\_\text{In}_x\text{Ga}_{1-x}\text{As}_{1-y}\text{N}_y}^s}, \tag{9}$$

where Q_v is the valence band offset (VBO) ratio of the heterostructure. ΔE_g^s represents the difference of the strained band-gap energy between the respective materials in the parentheses, and Δ_v^s represents the difference of the amount of valence band edge shift introduced by strain between the respective materials in the parentheses. $E_{g\_\text{AlAs}}^s$ and $E_{g\_\text{In}_x\text{Ga}_{1-x}\text{As}_{1-y}\text{N}_y}^s$ are the band-gap energy of AlAs and $\text{In}_x\text{Ga}_{1-x}\text{As}_{1-y}\text{N}_y$ considering strain, respectively.

C. Effects of the electric field

Within the framework of the eight-band $k \cdot p$ model, the overall eight-band Hamiltonian taking electric field into account is given by

$$H'\Phi = E\Phi, \tag{10}$$

where

$$H' = H_0 + V_F(z), \tag{11}$$

where H_0 is the full 8×8 Hamiltonian without electric field, which is given as

$$H_0 = H_k + H_s + V_{\text{conf}}(z), \tag{12}$$

where H_k is the unstrained 8×8 Hamiltonian, H_s is the 8×8 strain matrix, and the diagonal matrix $V_{\text{conf}}(z)$ describes the potential profiles in the z direction with discontinuities at the interface due to the CBO and VBO.[11] In Eq. (11), we use $V_F(z)$ to indicate the electric field distribution along the growth direction, which can be expressed as

$$V_F(z) = -eFz, \tag{13}$$

where e is the electron charge, F represents the strength of an external electric field, z is the coordinate in the growth direction along the CQW, and the origin of the electric field potential is taken as the midpoint of the second well. For con-

venience, throughout the work, the positive bias polarity corresponds to the CB potential being lowered along the growth direction z, as shown in Fig. 1.

III. RESULTS AND DISCUSSIONS

In order to verify our theoretical model for the calculations in the QCL structures, we have performed some calculations based on the eight-band model and compared them with the experimental and theoretical results reported in the literatures. The results are presented in Fig. 2 and Table II. Figure 2 shows our calculation on the GaAs/AlGaAs QCL structure which was demonstrated by Sirtori et al.[7] The com-
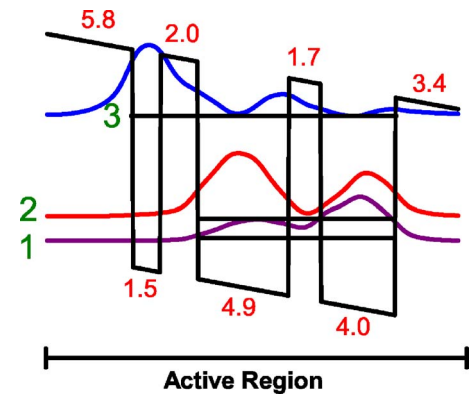

FIG. 2. (Color online) Comparison of the active region of the laser heterostructure at threshold bias (at 48 kV/cm) between the results of our calculation and Ref. 7. Shown are the positions of the calculated energy subbands and the corresponding modulus squared of the wave functions, denoted by flat solid lines and curved solid lines, respectively. The material system considered is GaAs/Al$_{0.33}$Ga$_{0.67}$As CQWs. Numbers 1, 2, and 3 indicate the sequence of electron states, E_1, E_2, and E_3, respectively. The sequence of the wells and barriers is in accordance with the definitions from Fig. 1. The thicknesses of the layers are in unit of nm. The calculated transition energies by the eight-band model are $E_{32}=143$ meV and $E_{21}=38$ meV.

TABLE II. Comparison of theoretical transition energies of GaAs/AlGaAs by the eight-band $k \cdot p$ model with published values.

Barrier layer composition (Al)	Well and barrier widths (wells 1, 2, and 3 and barriers 1, 2, and 3) (nm)	External electric field (kV/cm)	Our calc. E_{32} (1) (meV)	Publ. E_{32} (2) (meV)	Difference (1)–(2) (meV)
1[a]	3.3,6.8,6.0 0.5,0.5,3.0	39	127	109	18
0.33[b]	1.5,4.9,4.0 2.0,1.7,11.4	45	139	130	9
0.45[c]	1.9,5.4,4.8 1.1,1.1,7.4	48	147	160	−13
0.45[d]	4.3,5.0,5.4 0.94,0.94,2.84	30 40	35 47	43 56	−8 −9

[a]Reference 9.
[b]Reference 19.
[c]Reference 13.
[d]Reference 20.

parison is made on the first three principal electron states that are confined in the active region, which comprises of wells 1–3 (equal to 15, 49, and 40 Å, respectively) and barriers 1–3 (equal to 20, 17, and 92 Å, respectively). Our calculated transition energy from the upper lasing level (E_3) to the lower lasing level (E_2) for laser action, namely, E_{32}, equals to 143 meV. And the transition energy from the lower lasing level (E_2) to the ground level (E_1), namely, E_{21}, equals to 35 meV. These values are in agreement with the measured E_{32} (132 meV) and their calculated E_{21} (35 meV) in Ref. 7. Also, as can be seen from Fig. 2, the respective squared wave functions calculated are also in accordance with the published results. In Table II, the comparisons of our predicted transition energy E_{32} with the published results on GaAs/Al$_x$Ga$_{1-x}$As QCLs establish the reliability of our method.[9,13,19,20]

Figure 3 illustrates the conduction band diagram of one period of the QCL active region in the laser core. It consists of three In$_{0.3}$Ga$_{0.7}$As$_{0.97}$N$_{0.03}$ quantum wells closely coupled
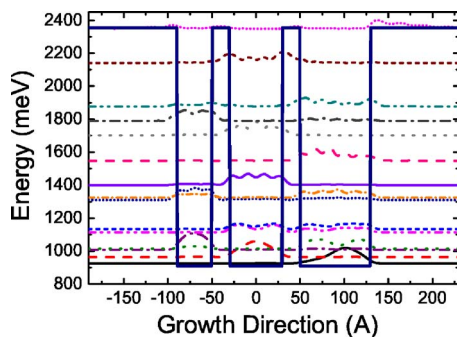

FIG. 3. (Color online) Schematic conduction band diagrams and the modulus squared of the bound state wave functions of a single period of the In$_{0.3}$Ga$_{0.7}$As$_{0.97}$N$_{0.03}$/AlAs coupled quantum well, which is the same as an active region of the quantum cascade laser structure, under zero bias. The InGaAsN wells have thicknesses of 40, 60, and 80 Å from left to right and are separated by 20 Å AlAs barriers (bw1 and bw2). The outmost barrier (bw3) is 200 Å altogether. The energy levels corresponding to the individual wave function counted from the lowest energy to the highest energy are E_1 to E_{15}. The temperature is 300 K.

by AlAs barriers. The zero point of the potential is taken as the valence band maximum (VBM) without strain. The same definitions hold for the following discussions. The temperature and electric field strength being considered are 300 K and 0 kV/cm, respectively. The eigenstates are calculated by solving Eq. (1) using the eight-band $k \cdot p$ method. As can be observed from the figure, there are overall 15 subbands plotted, with 14 bound states and 1 quasicontinuum state just above the barriers. In all cases, we express the nth subband in the wth well of the three-coupled wells in terms of C_n^w. For instance, the first subband confined in well 3 is expressed as C_1^3. Thus, by applying the definition C_n^w, the first five states in the TQWs are E_1-C_1^3, E_2-C_1^2, E_3-C_1^1, E_4-C_2^3, and E_5-C_2^2. Such an order of the levels is the consequence of the linear function form that the subband energy decreases as the well width increases. As the diagram indicates, the 80 Å well is the widest, thus the ground electron state of the whole CQWs is confined in this well. The second electron state is confined in the second widest well, 60 Å central well, and the third state is confined in the narrowest well, and so forth. As In and N concentrations increase to 30% and 3%, respectively, the CBO of the heterostructure increases to 1.5 eV. At the same time, the CB effective mass of In$_x$Ga$_{1-x}$As$_{1-y}$N$_y$ increases with the nitrogen concentration. Consequently, the subbands in the CQWs become closer and lower. By utilizing this regime, it is possible to design such a QCL structure, within which the upper lasing level will be lower than the X point in the CB of the barrier, in order to avoid the Γ-X intervalley transition. Moreover, a deeper well leads to the freedom in enlargement of the separation between the upper lasing level (E_3) and the lower lasing level (E_2), which is promising for 3−5 μm QCL design.

The subband and transition energy of the QCL active region calculated as a function of the width of well 1 (10−60 Å) is presented in Fig. 4(a). As can be seen from the figure, as well 1 grows, E_1 gradually increases from 1215 to 1228 meV, and E_2 slightly increases from 1246 to 1248 meV, nearly unaltered, whereas E_3 reaches a
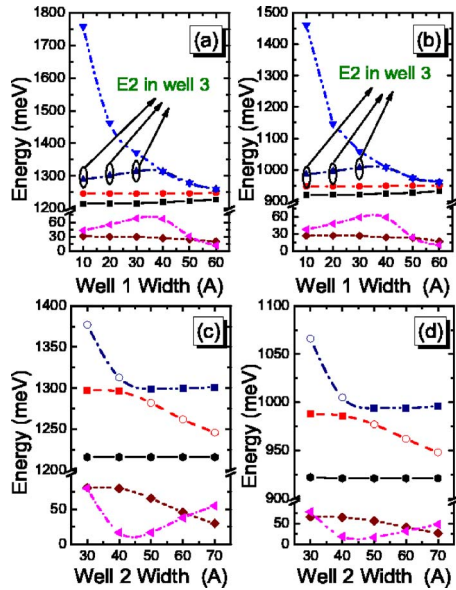
FIG. 4. (Color online) Dependence of subband and transition energy for active regions on [(a) and (b)] well 1 widths and [(c) and (d)] well 2 widths. The subband energy are shown above the break, counted from bottom to the top, they are E_1 (solid line), E_2 (dashed line), E_3 (dashed dotted line), and the first subband being confined in well 1 [dashed dotted line, which is only for (a) and (b)]. While below the break, the transition energy is shown. The bottom two curves are E_{21} (short dashed line) and E_{32} (short dashed dotted line). Note that there are some differences in the data points along the first two subband energy curves from the top of (c) and (d): (■) denotes that the electron states are the second one of well 3, and (○) denotes that they are the first energy levels of well 2. (a) and (c) are the results of $In_{0.1}Ga_{0.9}As_{0.99}N_{0.01}$/AlAs CQWs, with (a) ww2=70 Å, ww3=80 Å, bw1,2=20 Å, and bw3=200 Å, while (c) ww1=20 Å, ww3=80 Å, bw1,2=20 Å, and bw3=200 Å. (b) and (d) are the results of $In_{0.3}Ga_{0.7}As_{0.97}N_{0.03}$/AlAs CQWs, with (b) having the same QW structure with (a) and (d) having the same QW structure with (c). All the calculations are under no electric field and room temperature.

maximum at the well width of 40 Å; furthermore, a decrease at larger well widths is observed. The topmost curve shows that C_1^1 falls with the width of well 1, supporting the notion that the larger the well width, the lower the confined energy is. It is more interesting to note the trend of the E_3 curve, which changes from an increase to a decrease when ww1 =40 Å. It is due to the fact that when ww1=40 Å, C_1^1 alternates with C_2^3 to be E_3. Another interesting thing to note is that with the widening of well 1, E_1 and E_2 do not decrease but increase instead. It can be explained as follows: the order of energy levels localized in the whole CQW region is heavily impacted by the coupling effect, which causes the discrete levels localized in wells 2 and 3 to rise slightly with the increasing well 1 width. On the contrary, the energy levels in well 1 drop with the increasing well 1 width. The trend continues until C_1^1 becomes even lower than C_2^3, which pushes C_2^3 to rise slowly. It follows that C_1^3 in the same well as C_2^3, e.g., E_1 increases. For the case of E_2, since C_1^2 is lower than C_2^3, while C_1^1 is close to C_2^3, the drop of C_1^1 has negligible effect on C_1^2. Moreover, since well 2 is located at the center of the CQW, the two wells located on the either side have contrary coupling effect on it, which means that C_1^3, C_2^3, and C_1^1 will push the state to increase dramatically slower than the levels in well 3 and, therefore, a nearly unchanged E_2 state results. Following the trend of the discrete levels

versus the width of well 1, the transition energy E_{32} first increases and then decreases, while the transition energy E_{21} decreases with the increasing well 1 width, as Fig. 4(a) indicates. The points made so far apply in principle to Fig. 4(b), which is calculated with In=30% and N=3%; all the other conditions are the same.

The subband and transition energy of the QCL active region calculated as a function of the width of well 2 (30–70 Å) are depicted in Fig. 4(c). As sketched in the figure, as ww2 widens, E_1 is fixed, E_2 drops, and E_3 decreases at first and then rises slightly. The different symbols used in the same curve show that the electron states are not confined in the same well for the same energy level. For the E_2 curve, the first two points represent C_2^3 and the others represent C_1^2. For the E_3 curve, the first two points represent C_1^2 and the others represent C_2^3. This is a result of that at first, C_1^2 is higher than C_2^3, thus the former energy designates E_3 and the latter designates E_2, as the well 2 width increases, and C_1^2 drops until it is lower than C_2^3. This leads to the exchanging of the levels localized in the whole CQW region. If one only looks at the variation of C_1^2 as ww2 widens, it decreases straightly. While for the variation of C_2^3, the amount is negligible. Because C_1^3 is far lower than the other states, it is unaffected by the other states as the well 2 width becomes larger; therefore E_1 is fixed all throughout the process. From the analysis above, the transition energy for E_{32} drops at first and then rises, while the transition energy for E_{21} decreases as the width of well 2 increases, as indicated in Fig. 4(c). So is the case in Fig. 4(d), when In=30% and N=3%.

Let us now examine how the width of well 3 affects the CB structure of the $In_{0.1}Ga_{0.9}As_{0.99}N_{0.01}$/AlAs CQWs. As illustrated in Fig. 5(a), E_1 decreases monotonously with the well 3 width, owing to the fact that throughout the range of ww3, C_1^3 is E_1 of whole the system. As ww3 grows, C_1^3 (E_1) drops. The relationship between E_2, E_3, and ww3 is a little more complicated. E_2 initially remains unchanged until ww3=70 Å, where it begins to decrease markedly. It could be explained that when ww3 is less than 70 Å, E_2 is localized in well 2. The fixed well width of well 2 results in a fixed E_2 energy. However, in the range that ww3 is beyond 70 Å, E_2 turns to be C_2^3, and as ww3 continues to increase, E_2 drops simultaneously. As for the case of E_3 vs ww3, as the latter grows, the E_3 curve drops at first and then keeps flat. It happens because when ww3=40 Å, C_1^1 is E_3. With an increase in ww3, the energy of C_2^3 falls below C_1^1 and substitutes its position for the whole system, which means that, when well 3 is larger than 50 Å, E_3 is localized in well 3. As can be observed in Fig. 5(a), E_3 decreases with the increasing ww3, until ww3 equals to 70 Å, and C_2^3 falls below C_1^2. From then on, C_1^2 becomes E_3. Because no variation of the well width occurs in well 2 since then, the E_3 curve keeps flat. As a result of the variation of each subband as the ww3 increases, an initial increase followed by a decrease occurs in E_{21} and the contrary trend occurs in E_{32}, as depicted in Fig. 5(a). The same discussions apply to the similar case when In=30% and N=3%, as shown in Fig. 5(b).

After investigating the impact of well widths on the band structure of $In_xGa_{1-x}As_{1-y}N_y$/AlAs QCL active region, we are interested to know how the In and N concentrations
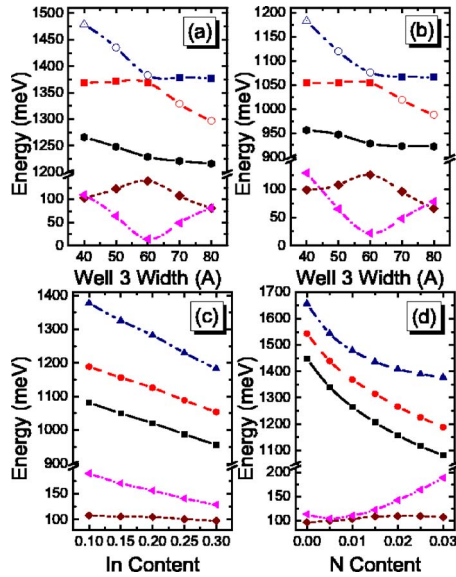
FIG. 5. (Color online) Dependence of subband energy and transition energy for active regions on [(a) and (b)] well 3 widths, (c) indium composition, and (d) nitrogen composition. Same legend from Figs. 4(c) and 4(d) applies. Note that there are some differences in the data points along the first two subband energy curves from the top of (a) and (b): ($\triangle$) designates the ground state of well 1, ($\bigcirc$) designates that the electron states are the second ones of well 3, and ($\blacksquare$) designates the first energy levels of well 2. (a) and (b) are the results of $In_{0.1}Ga_{0.9}As_{0.99}N_{0.01}$/AlAs and $In_{0.3}Ga_{0.7}As_{0.97}N_{0.03}$/AlAs CQWs, respectively, with ww1=20 Å, ww2 =30 Å, bw1,2=20 Å, and bw3=200 Å. (c) and (d) are N_w=3% and In_w =10%, respectively, with ww1=20 Å, ww2=30 Å, ww3=40 Å, bw1,2 =20 Å, and bw3=200 Å. All the calculations are under no electric field and room temperature.

could impact on the band structure. The results are plotted in Figs. 5(c) and 5(d). As can be observed from Fig. 5(c), with indium atoms being added, the first three subband energies of the system monotonously decrease. It is due to the fact that as the In content grows, the band gap of $In_xGa_{1-x}As_{0.97}N_{0.03}$ decreases, which directly leads to the localized levels in the CB fall. With respect to the transition energy, we can see that E_{21} slightly decreases while E_{32} decreases dramatically. One thing to note is that the energy levels E_1, E_2, and E_3 corresponding to all the In concentrations are concentrated in ww3, ww2, and ww1, respectively. E_{21} corresponds to the energy difference between C_1^3 and C_1^2, and E_{32} corresponds to the energy difference between C_1^2 and C_1^1. There are two reasons why E_{32} drops faster than E_{21}. (1) The higher the energy, the faster it drops; hence, the dropping velocity of each subband is in the order of $E_3 > E_2 > E_1$. (2) With a rise in the In content, the CBO becomes larger. As a result, more and more electron states are incorporated into the CBO, which pushes the other subbands to be further lowered. The amount of the decrease is in the order of $E_3 > E_2 > E_1$. Rules (1) and (2) make it clear that E_{32} falls more rapidly than E_{21}. Figure 5(d) shows the dependence of band structure on the nitrogen composition. With an increasing N content, E_1, E_2, and E_3 decrease simultaneously. It arises from the decrease of InGaAsN band-gap energy with increasing nitrogen atoms. However, this variation is not the same as that of the In concentration, which decreases nearly linearly. This is because our calculation is based on the BAC model, in which the band gap of InGaAsN does not decrease linearly but

gradually with N concentration, as can be seen from our summary in Ref. 11. The slow decreases of both E_2 and E_1 lead to a trivial increase of E_{21}. What is more interesting is that the energy separation between E_3 and E_2 slightly decreases at first and then increases sharply. This can be attributed to the special effect of the nitrogen related band, which is located at about 1500–1600 meV, near E_3. Thus the impact of nitrogen band on E_3 is much more obvious than that on the E_2 band, which causes E_3 to decrease more slowly than E_2 and E_1, and results in an increase in E_{32}.

Our initial attempt on the design of 3–5 μm QCL emission with the $In_xGa_{1-x}As_{1-y}N_y$/AlAs CQW structure is based on the following: (1) In content ranging from 0% to 30%, (2) N content ranging from 0% to 3%, (3) ww1 ranging between 10 and 60 Å, (4) ww2 ranging between 20 and 70 Å, and (5) ww3 ranging between 30 and 80 Å. At the same time, taking ww1 < ww2 < ww3, bw1=bw2=20 Å, bw3=200 Å, T =300 K, and F=0 kV/cm. However, the calculated results tell us that there is no combination within this range that reaches the desired 3–5 μm laser emission. One should note that we have not yet attempted to design the QCL structures by taking ww1 < ww2 and ww1 < ww3, at the same time, allowing ww2 > ww3. Such a combination has been adopted extensively in QCL research over the past few years.[1,7] Let us now try to extend our design by ranging ww1 from 10 to 20 Å, ww2 from 30 to 60 Å, and ww3 from 25 to 55 Å. All the other parameters are taken as in the first design plot mentioned above. As a result, though a large number of the calculations with In content below 20% can achieve the laser emissions within 3–5 μm, the corresponding E_3 level is either much higher than or close to the conduction band edge at X point of the AlAs barrier, which could deteriorate the QCL performance as electrons could transit from the Γ valley in the well layers into the X valley in the barriers. After a detailed investigation, we found that such a combination of $In_{0.2}Ga_{0.8}As_{0.97}N_{0.03}$/AlAs CQW with ww1=10 Å, ww2=35 Å, ww3=27 Å, bw1=bw2=20 Å, and bw3=200 Å could reach the result of E_{32}=313 meV (3.96 μm). Additionally, E_3 can be made equal to 1418 meV, which is below the conduction band edge in the X valley of AlAs barrier (1505 meV), satisfying our requirements.

The aim to achieve the shortest emission wavelength leads us further into a consideration of the dependence of transition energy on the barrier width, electric field, and temperature, with the optimum combination so far derived. As shown in Fig. 6(a), we investigate how bw1 and bw2 will affect the transition energy. With the bw1 (bw2) ranging from 10 to 30 Å, E_1 first rises and then falls slightly, E_2 decreases at first and then increases a little, and E_3 exhibits an increase. That is due to the order rearranging of the discrete subbands in different wells, and similar discussions have been made before. The variations in the subband energies lead to that E_{21} decreases quickly at first and then increases slightly; on the contrary, E_{32} grows at first and then drops slowly with bw1 (bw2). As a result, an optimal bw1 (bw2) =24 Å has been obtained, with the other parameters being
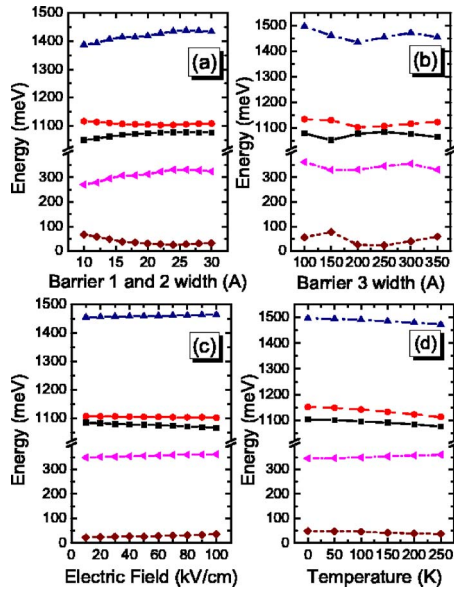
FIG. 6. (Color online) Dependence of subband energy and transition energy for active regions on (a) barrier 1,2 widths, (b) barrier 3 widths, (c) electric field, and (d) temperature. Same legend from Figs. 4(c) and 4(d) applies. Shown are the results of $In_{0.2}Ga_{0.8}As_{0.97}N_{0.03}$/AlAs CQWs with ww1 =10 Å, ww2=35 Å, and ww3=27 Å. Meanwhile set (a) bw3=200 Å, (b) bw1,2=22 Å, and [(c) and (d)] bw1,2=24 Å and bw3=250 Å. (a)–(c) are calculated at 300 K and (a) and (b) are calculated under $F=0$ kV/cm, while (c) is calculated under 100 kV/cm electric field.

mentioned in the figure caption. The corresponding E_{32} rises from 313 meV when bw1 (bw2)=20 Å to 331 meV when bw1 (bw2)=24 Å, as depicted in Fig. 6(a).

We have also plotted energy levels versus bw3 in Fig. 6(b). In the range of 100–350 Å, the trends of the energy curves are complicated due to the fast changing of their localized wells. Whereas, in addition to achieve the largest E_{32}, it is important to bear in mind that E_3 should be as small as possible. The compromise results in an optimal combination with bw3 being 250 Å (other parameters are the same as stated in the previous step). The increase of bw3 to 250 Å corresponds to an enhancement of E_{32} to 346 meV. Meanwhile, the calculated E_3 is 1454 meV (below CB edge of the X valley in the AlAs layer).

Figure 6(c) shows the calculated energy levels and separations as a function of the electric field strength for the CQW structures. To achieve a successful QCL emission, E_{21} should match the optical phonon energy in order to achieve the maximum population inversion. E_{21} corresponding to the best combination so far achieved is 23 meV; however, it is smaller than E_{phonon} for $In_{0.2}Ga_{0.8}As_{0.97}N_{0.03}$ (36 meV). Therefore, we further investigate how the external electric field impacts on the band structure. As depicted in Fig. 6(c), as F increases, E_1 decreases, E_2 slightly decreases (nearly unchanged), and E_3 increases. Consequently, the curves exhibit linear stark effects, e.g., E_{21} increases dramatically while E_{32} increases slightly (both with respect to their extent) with the electric field strength. Thereby when F =100 kV/cm, a largest E_{32} of 362 meV is obtained. Additionally, E_{21} reaches 36 meV, which is just our desired value.

We have also done research on energy level and its separation as a function of temperature, as shown in Fig. 6(d). All
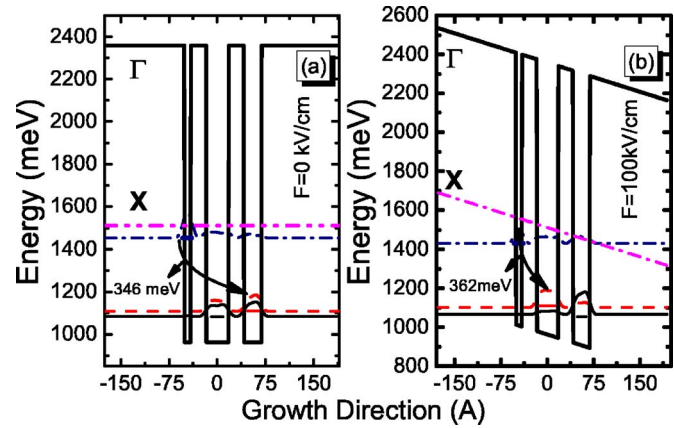

FIG. 7. (Color online) Conduction band profiles of the active regions for a ww1=10 Å, ww2=35 Å, ww3=27 Å, bw1,2=24 Å, and bw3=250 Å $In_{0.2}Ga_{0.8}As_{0.97}N_{0.03}$/AlAs QCL structure under applied electric fields of (a) 0 and (b) 100 kV/cm at room temperature. The subband energy is sketched as the flat solid line. The moduli squared of the relevant wave functions are shown, counted from bottom to the top, they are E_1 (solid line), E_2 (dashed line), and E_3 (dashed dotted line). The arrows in (a) and (b) indicate the lasing action related transition energy E_{32}. Dashed dotted lines denote the conduction band at X point.

of the first three electron states and the separation between the first two subbands drop, while the separation between the upper lasing level and the lower lasing level decreases as the temperature increases. It can be explained as that the temperature sinking induces the band gap of $In_xGa_{1-x}As_{1-y}N_y$ to reduce, which leads to the declining subband energy.

Finally, the band structure of our optimized combination is plotted in Fig. 7. Figure 7(a) is the structure under no external electric field and Fig. 7(b) is the structure at 100 kV/cm bias. As can be observed from Fig. 7(a), when no electric field added, E_{21} and E_{32} are 23 and 346 meV, respectively. E_3 equals to 1454 meV, which is below the X valley CB edge of the barrier. Figure 7(b) tells us that the intersubband transition energy E_{21} (36 meV) is in accordance with E_{phonon} and a 362 meV transition from E_3 to E_2 can be obtained under an electric field of 100 kV/cm. E_3 (1464 meV) is below the CB edge located in the X valley of AlAs barrier (1505 meV), which fulfills our design requirements.

IV. CONCLUSIONS

In conclusion, the calculation and design of the active region of $In_xGa_{1-x}As_{1-y}N_y$/AlAs QCLs have been reported within the eight-band $k \cdot p$ scheme. This material system is very promising for the production of QCLs operating in the $\lambda \sim 3-5$ μm atmospheric window thanks to its large conduction band offset. The dependence of conduction band structure on well widths, barrier widths, In concentration, N concentration, electric field strength, and temperature has been investigated. A linear Stark effect occurs when an electric field is applied, which can be utilized for fine tuning the emission wavelength and population inversion. By a careful tailoring of the layer thicknesses and compositions, an optimal structure comprising of $In_{0.2}Ga_{0.8}As_{0.97}N_{0.03}$/AlAs CQW with ww1=10 Å, ww2=35 Å, ww3=27 Å, bw1=bw2 =24 Å, and bw3=250 Å has been obtained. As anticipated,

this system can emit at a wavelength of 3.4 μm under an electric field of 100 kV/cm and at room temperature. The system could avoid the detrimental $\Gamma - X$ intervalley interaction, because its upper lasing level is lower than the conduction band edge in the X valley of the particular AlAs barrier. This work is useful for the InGaAsN/AlAs QCLs design.

ACKNOWLEDGMENT

[1] J. Faist, F. Capasso, D. L. Sivco, C. Sirtori, A. L. Hutchinson, and A. Y. Cho, Science **264**, 553 (1994).

[2] J. S. Yu, S. Slivken, A. Evans, L. Doris, and M. Razeghi, Appl. Phys. Lett. **83**, 2503 (2003).

[3] M. Beck, D. Hofstetter, T. Aellen, J. Faist, U. Oesterle, M. Ilegems, E. Gini, and H. Melchior, Science **295**, 301 (2002).

[4] D. G. Revin, L. R. Wilson, E. A. Zibik, R. P. Green, J. W. Cockburn, M. J. Steer, R. J. Airey, and M. Hopkinson, Appl. Phys. Lett. **85**, 3992 (2004).

[5] Q. Yang, C. Manz, W. Bronner, C. Mann, L. Kirste, K. Kohler, and J. Wagner, Appl. Phys. Lett. **86**, 131107 (2005).

[6] C. Beck, I. Prevot, X. Marcadet, B. Vinter, and C. Sirtori, Appl. Phys. Lett. **78**, 1029 (2001).

[7] C. Sirtori, P. Kruck, S. Barbieri, P. Collot, J. Nagle, M. Beck, J. Faist, and U. Oesterle, Appl. Phys. Lett. **73**, 3486 (1998).

[8] D. Scalari, S. Blaser, J. Faist, H. Beere, E. Linfield, D. Ritchie, and G. Davies, Phys. Rev. Lett. **93**, 237403 (2004).

[9] C. Becker, C. Sirtori, H. Page, G. Glastre, V. Ortiz, X. Marcadet, M. Stellmacher, and J. Nagie, Appl. Phys. Lett. **77**, 463 (2000).

[10] C. P. Garcia, A. D. Nardis, V. Pellegrini, J. M. Jancu, and F. Beltram, Appl. Phys. Lett. **77**, 3767 (2000).

[11] S. T. Ng, W. J. Fan, Y. X. Dang, and S. F. Yoon, Phys. Rev. B **72**, 115341 (2005).

[12] M. Galluppi, L. Geelhaar, and H. Riechert, Appl. Phys. Lett. **86**, 131925 (2005).

[13] H. Page, C. Becker, A. Robertson, G. Glastre, V. Ortiz, and C. Sirtori, Appl. Phys. Lett. **78**, 3529 (2001).

[14] Y. X. Dang, W. J. Fan, S. T. Ng, S. F. Yoon, and D. H. Zhang, J. Appl. Phys. **97**, 103718 (2005).

[15] Y. X. Dang, W. J. Fan, S. T. Ng, S. Wicaksono, S. F. Yoon, and D. H. Zhang, J. Appl. Phys. **98**, 026102 (2005).

[16] I. Vurgaftman, J. R. Meyer, and L. R. Ram-Mohan, J. Appl. Phys. **89**, 5815 (2001).

[17] I. Vurgaftman and J. R. Meyer, J. Appl. Phys. **94**, 3675 (2003).

[18] D. J. Arent, Phys. Rev. B **41**, 9843 (1990).

[19] S. Barbieri, C. Sirtori, H. Page, M. Stellmacher, and J. Nagle, Appl. Phys. Lett. **78**, 282 (2001).

[20] C. Pflugi, W. Schrenk, S. Anders, G. Strasser, C. Becker, C. Sirtori, Y. Bonetti, and A. Muller, Appl. Phys. Lett. **83**, 4698 (2003).